Pyrene and Biochar (Raman Spectroscopy)

Amelia Carolina Sparavigna

Department of Applied Science and Technology, Polytechnic University of Turin, Italy

Email: amelia.sparavigna@polito.it

Pyrene is a polycyclic aromatic hydrocarbon (PAH) organic compound. Here we consider its Raman spectroscopy, and how it is revealing, when used to create nanograins (Gavilan et al., 2022), a spectrum which is like that we can observe when biochar is investigated. Besides the approach by Gavilan and coworkers, the research by Smith et al., 2016, based on the Raman spectra of several PAH compounds, and proposed to determine an assignment for the bands of char, will be considered too.

Keywords: Raman spectroscopy, Pyrene, PAHs, Biochar, Char.

Introduction

Pyrene is a single, well-defined molecule, made of four fused benzene rings. It is a polycyclic aromatic hydrocarbon (PAH) molecule, which can be obtained by means of various processes, including the incomplete combustion of organic matter (such as wood and tobacco) and the photoionization of larger hydrocarbons, as it happens in the interstellar space (Gavilan et al., 2022). Pyrene photoionization is studied to understand its electronic structure and for the development of new materials (Figueira-Duarte & Mullen, 2011). Let us remember that pyrene is a pollutant, and it can be found in air, water, and soil (Bömmel et al., 2000), released into the environment because of industrial activities and burning of fossil fuels. Here we illustrate some Raman spectra of Pyrene. We will see that Gavilan et al., 2022, in the case of pyrene generated nanograins, obtained a spectrum which looks like that of biochar. We will also consider the results obtained by Smith et al., 2016, about their proposal of a structural analysis of char made by means of Raman spectroscopy.

Pyrene

As told by Gavilan et al., 2022, PAHs are a class of aromatic organic molecules that are ubiquitous on Earth, in the solar system, and in the interstellar medium. PAHs are playing "important roles in the evolution of the cosmic environments" (Gavilan et al., 2022). Pyrene ($C_{16}H_{10}$), is the “smallest peri-condensed polycyclic aromatic hydrocarbon (PAH)”. Gavilan and coworkers used Raman spectroscopy to characterize pyrene in microcrystals and in pyrene-derived nanograins. The researchers observed a spectrum of microcrystalline pyrene which consisted of narrow bands, in agreement with measurements of single and powder pyrene crystals. The Table 2 of the work by Gavilan et al., gives the most relevant peaks at (cm^{-1}):

Gavilan et al. *405.5, 590.0, 1064.0, 1141.0, 1239.0, 1404.0, 1592.0, 1626.0, 1641.0*

Gavilan and coworkers compared their results to those obtained by Bree et al., 1971, and Cloutis et al., 2016. Here in the following, the corresponding bands:

Bree et al. *408, 593, 1067, 1144, 1243, 1408, 1596, 1630, 1644*

Cloutis et al. *409, 595, 1067, 1142, 1241, 1407, 1594, 1629, 1643*

In Smith et al. 2016, the band of pyrene are given as (cm^{-1}):

Smith et al. *1066 1241 1407 1595 1628*

At the web page of RAMDB, we can find further pyrene Raman spectra. As explained by Mattioda et al., 2024, "the NASA Raman Spectroscopic Database (Ramdb) was developed to provide a publicly accessible, user-friendly database for spectra relevant to the planetary science community".

In the article by Gavilan et al., it is stressed that the bands centered at 1239 and 1404 cm^{-1} have a "red shoulder near their base". The line profiles can be not symmetric "due to different sizes of crystallites, which arise from a heterogeneous crystallite size distribution after sample preparation. Smaller crystallites could also result in more asymmetric line profiles" (Gavilan et al., mentioning Richter et al., 1981, Campbell & Fauchet, 1986).

For comparison, besides the results given by Gavilan et al., 2022, Bree et al., 1971, Cloutis et al., 2016, and Smith et al., 2016, let us mention Gu et al., 2013, where we can find SERS investigation for pyrene giving seven distinctive bands (cm^{-1}):

Gu et al. *405, 594, 1241, 1408, 1596, 1628, 1648*

Gu and coworkers explain that the spectrum can be divided into five regions: (1) 1650–1500 cm^{-1}, characterized by the "C–C stretching mode mixed with some CH in-plane bending vibrations"; (2) 1500–1350 cm^{-1}, a region which is containing the bands that are due to the "strong C–C stretching coupled with weak ring-breathing vibrations"; (3) 1300–1000 cm^{-1}, it is the region where the bands are produced mainly by "CH in-plane bending vibrations"; (4) 1000–600 cm^{-1}, in this case the bands are coming from the "CH out-of-plane bends". Finally (5), it is the region consisting of the spectrum below 550 cm^{-1}, it "may be due to out-of-plane skeletal deformation vibrations" (Gu et al., 2013).

Returning to the measurements made by Gavilan et al., 2022, the researchers observed that in the case of pyrene-derived nanograins, that is, nanograins generated from gaseous pyrene, the spectrum shows a broad graphitic G band at 1587 cm^{-1} and multiple disorder D bands, with the largest peak at 1388 cm^{-1}. According to Gavilan and coworkers, the bands are attributed to defects in the carbonaceous structure. The researchers produced the nanograins in the COSmIC (Cosmic Simulation Chamber) facility at NASA Ames Research Center. The chamber is preparing solid carbonaceous samples from the gas phase pyrene. In the Figure 5 provided by Gavilan and coworkers we can see the baseline-corrected Raman spectrum of COSmIC nanograins. The Raman spectrum is decomposed by Gavilan and coworkers, using Lorentzian and Gaussian profiles; the decomposition is "revealing the presence of a G band and multiple D bands". In the Fig.1 we propose a sketch of the pyrene-generated nanograins spectrum.

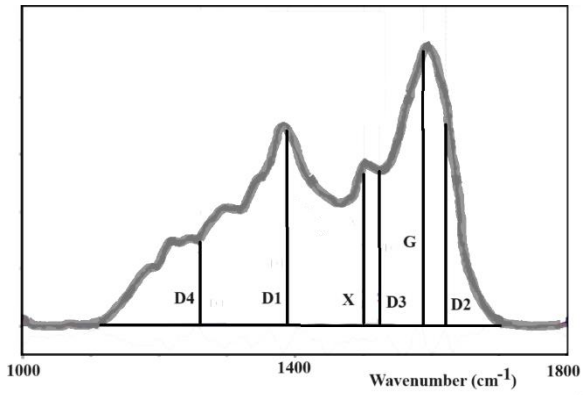

Fig.1: This sketch is made to illustrate the Raman spectrum proposed by Gavilan et al., 2022, in their Figure 5. The grey line is giving the data obtained from COSmIC pyrene-generated nanograins. Using Lorentzian and Gaussian components, Gavilan and coworkers determined six bands; the positions of their centers are here given by the black lines. In general, the decomposition of Raman spectra can be improved by using q-Gaussians, instead of Lorentzian and Gaussian functions (see Sparavigna, 2023, 2024).

Gavilan et al., 2022, used Lorentzian profiles for D_1, D_2, X and G, whereas a Gaussian profile was used for D_2 and D_3. Let us note that, if instead of using Gaussians and Lorentzian profiles in a decomposition of Raman spectrum, we use q-Gaussians or other profiles (such as Voigt or pseudo-Voigt profiles), the result can change in the number and position of peaks.

Gavilan and coworkers tell that "Raman spectroscopic studies of different nanostructured carbonaceous materials, including pristine and disordered graphite, carbon black, carbon nanotubes, charcoal, and soot have identified multiple D bands in addition to the single G band" (the mentioned articles are those by Al-Jishi and Dresselhaus, 1982, Brunetto et al., 2009, Dippel et al., 1999, Dresselhaus et al.,2005, Inoue et al., 2017, Jawhari et al., 1990, Sadezky et al., 2005, Tuinstra and Koenig, 1970. To explain the bands, Gavilan and coworkers add that the G band, ~1580 cm^{-1}, is due to the ideal graphitic lattice, the D_1 and D_2 bands, ~1350 and 1620 cm^{-1} respectively, are due to the disordered graphitic lattice. The origin of the D_3 band, ~1520 cm^{-1} is in the presence amorphous carbon. Then, "the D_4 band at ~1260 cm^{-1} is attributed to disordered graphitic lattice, polyenes and ionic impurities (mixed sp^2–sp^3 bonding), and generally C=C and/or C−C stretching modes" (Gavilan et al., 2022). The researchers add that "Currently, there is no consensus on the chemical significance of these so-called defect bands (i.e., D_2, D_3, and D_4)". Gavilan and coworkers are mentioning Vinogradoff et al., 2017.

Vinogradoff and coworkers, 2017, analyzed the Paris meteorite insoluble organic matter (IOM). "The Raman spectrum of the Paris IOM is typical of disordered carbons, with a composite G band ($G+D_2$) centered at 1585 cm^{-1}, a composite D band (D_1+D_4) centered at 1368 cm^{-1} and a D_3 band in between". Vinogradoff et al. are mentioning Ferrari and Robertson, 2000, Beyssac et al., 2003, and Bernard et al., 2010. "Note that there is no consensus on the exact physical or chemical significance of the so-called defect bands (D_1, D_2, D_3 and D_4)" (Vinogradoff et al., 2017, mentioning Beyssac and Lazzeri, 2012). Being the decomposition of the D-to-G Raman band depending on the choice of number and profile of components, a consensus on the significance of the bands is consequently difficult to be achieved. Regarding IOMs, Gavilan et al. found that the D-to-G Raman band values "for the pyrene nanograins match those from the highly disordered Allende meteoritic IOM best".

According to the experimental results given in the mentioned references, Gavilan and coworkers conclude that "The Raman spectrum of the COSmIC nanograins is typical of disordered carbons. A D band (D_1) is found centered at 1387 cm^{-1} , a composite G band ($G+D_2$) centered at 1588 cm^{-1} , and a D_3 band in-between at 1523 cm^{-1}". "The narrow X band in Table 3 can be attributed to a minor G (sp^2) band seen in graphitic amorphous carbons (Ferrari and Robertson, 2000) originating here from intermediate products of the growth of pyrene to larger PAHs in COSmIC" (Gavilan et al., 2022).

Of the D and G bands, we discussed in SSRN and ChemRxiv, where we considered the decomposition of the Raman spectrum made by means of q-Gaussian functions. The q-Gaussians are probability distributions having their origin in the framework of Tsallis statistics. A continuous real parameter q is characterizing them so that, in the range $1 < q < 3$, the q-functions pass from the usual Gaussian form, for q close to 1, to that of a heavy tailed distribution, at q close to 3. The value q=2 corresponds to the Cauchy-Lorentzian distribution. Among the experimental data investigated in SSRN and ChemRxiv , there are also those regarding biochar. Biochar (or simply char) is a substance obtained by heating organic material in a pyrolysis process. This process drives off volatile gases and liquids, leaving behind a stable carbon-rich solid material. Biochar is often referred to its potential benefit as soil amendment and for climate change mitigation (Beesley et al., 2011, Lehmann & Joseph, 2015, Azzi et al., 2022). It possesses a porous structure which is relevant for the soil health too (Sparavigna, 2023, Lee et al., 2022, Zhu et al., 2017). For what is regarding the climate change mitigation, biochar can be used to store carbon and reduce nitrous oxide emissions (Sohi, 2012, Cayuela et al., 2014, Wang et al., 2017). Being the biochar suitable for many applications, and for this reason known as the "black gold", the existence of toxic of cancerogenic substances in it is requiring a specific investigation. In fact, the "black gold" possesses a "dark side" (Godlewska et al., 2021). We will discuss this problematic aspect of biochar in a next work.

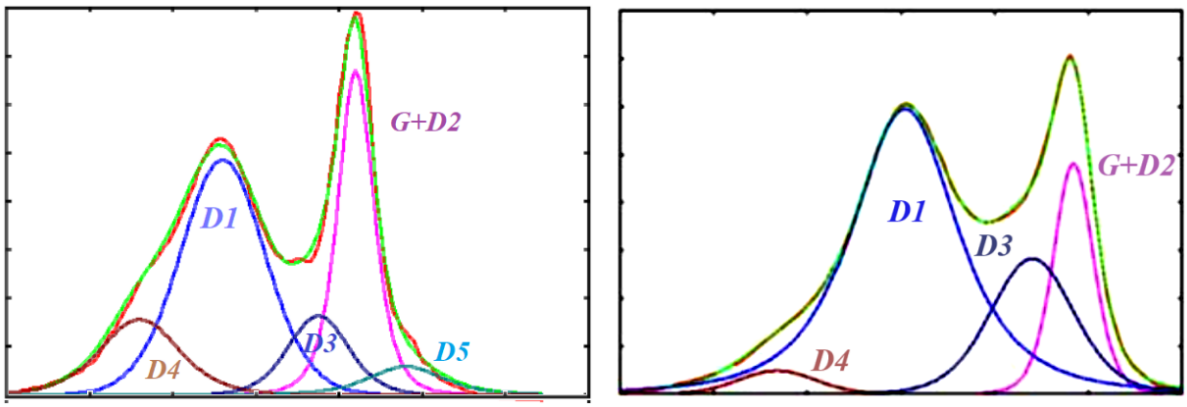

Fig. 2: The plot on the left is giving the decomposition obtained by means of 5 q-Gaussians, of a biochar D-to-G Raman spectrum available in the article by Sousa et al., 2020. The horizontal axis represents the Raman shift (arbitrary units). The D_2 band has been merged into G band. The green line is representing the fit, and the red line the data. Other colors are giving the q-Gaussian components. On the right, the plot is proposing a decomposition obtained by means of 4 q-Gaussians of data from Tagliaferro et al., 2020, regarding a biochar sample. Green (fit) and red (data) curves are almost indistinguishable.

In the Fig.2, two examples of D-to-G Raman spectra of biochar are proposed. The decomposition was made by means of q-Gaussian functions. A third example of (bio)char D-to-G Raman spectrum we will show in the Figure 3, from data by Smith et al., 2016. Besides investigating the pyrene Raman spectrum, Smith and coworkers analyzed naphthalene, perylene, benzo[a]pyrene, benzo[g,h,i]perylene, coronene and anhydrous tetracarboxylic perylene, by means of simulations and experimental results. Accordingly, they proposed a structural analysis of char for the D-to-G Raman spectrum. The approach proposed by Smith et al. was that of starting from single elements, with specific defects, to argue their presence in the Raman bands of char. The researchers concluded for ten bands. "Based on simulation results, a total of ten potential bands have been assigned between 1000 cm^{-1} and 1800 cm^{-1}. These

bands have been used to deconvolute a thermoseries of cellulose chars produced by pyrolysis at 300-700 °C" (Smith et al., 2016).

The char the researchers used for experiments was derived from cellulose and the Raman spectra of char produced at different temperature were given in Fig.11 of their article (Smith et al., 2016). By means of the deconvolution of these spectra, the researchers concluded that experiments were consistent with the "growth of PAH clusters, loss of oxygen, and development of non-hexagonal ring systems as pyrolysis temperature increased". As previously told, Smith and coworkers performed simulations to understand the role of defect and used the experimental spectra of the abovementioned compounds to validate the presence of Raman active vibrations in char.

"Key vibrational modes of various defects were analyzed for distinctive regions *to create a new series of band assignments* specifically tailored for chars produced at temperatures below 700 °C" (Smith et al., 2016). The researchers obtained a shoulder peak, about 1200 cm^{-1}, related to the vibrational modes for PAH structures, in particular of cycloheptane and larger ring systems. "The breathing modes of small PAHs (Naphthalene-pyrene scale) were found to be present between 1200 cm^{-1} and 1300 cm^{-1} as well as for larger ring systems (greater than coronene)". Moreover, Smith and coworkers consider "the valley commonly observed in Raman spectra and chars" consistent with the proposed models of disorder. For what is regarding the band between 1400 cm^{-1} and 1450 cm^{-1}, the researchers assigned it "to Kekulé dominated vibrational modes". The spectrum between 1480 cm^{-1} and 1550 cm^{-1}, that is the asymmetric G-band, is linked by Smith and coworkers "to coupling of breathing modes and asymmetric stretching caused by strained deformation within the PAH clusters and constriction of motion caused by oxygen inclusion" (Smith et al., 2016).

In the Figure 12 of the article by Smith et al., we can see a decomposition of one of the char Raman spectra. Smith and coworkers used seven Gaussians and a Lorentzian profile. Here in our Figure 3, we propose a sketch to illustrate the spectrum and the position of the centers of components.

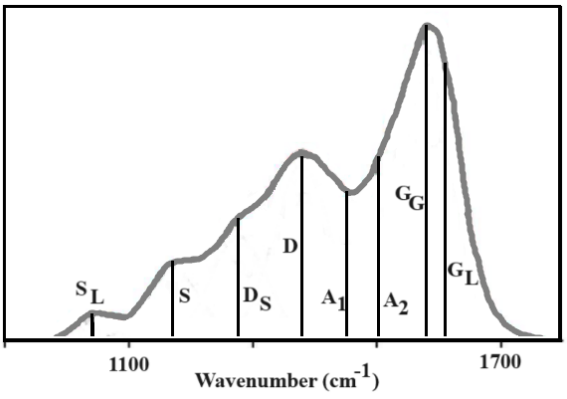

Fig.3: This sketch is made to illustrate a cellulose char Raman spectrum and its deconvolution in eight components (seven Gaussians and one Lorentzian profile G_L), proposed by Smith et al., 2016.

Smith and coworkers are proposing a detailed interpretation for the origin of the bands. For instance, S_L is the band corresponding to the breathing modes for small aromatic regions, whereas S is the breathing mode of the rings containing 7+ carbons, including benzene ring breathing modes. D_S represents the breathing modes for most PAHs, and D the combined breathing/Kekulé vibrations for PAHs. Then we have modes A_1 (breathing of 5-membered rings with Kekulé vibrations) and A_2 (breathing and asymmetric stretch vibrations of carbons near defects). G_G is the Gaussian distributed asymmetric vibrations for distribution of small PAHs, whereas G_L is the Lorentzian E_{2g} mode for large PAHs.

In the case of Smith and coworkers' approach, we have the bands defined according to the results of simulations and experiments regarding several PAH molecules. For Gavilan et al., 2022, the molecule that has been considered is that of pyrene. When pyrene-generated nanograins Raman spectrum is investigated, the bands mentioned by Gavilan et al., 2022, are those generally used for biochar, as discussed in SSRN. It is strictly necessary to note that the COSmIC chamber produced a remarkable "simulation" of char.

To conclude, let us stress once more that the number of components, such as the position of their centers, is depending on the profile used for the decomposition of the Raman spectrum. In Smith et al., 2016, the researchers used for simulations, and therefore for the subsequent conclusions, the Lorentzian profiles. Mentioning Sadezky et al., 2005, and Demtröder, 1982, Smith and coworkers proposed for char, as we can find in their Table IV and for the spectral range 975-1800 cm^{-1}, nine Gaussian bands and one Lorentzian band. Gavilan and coworkers too used Gaussian and Lorentzian profiles for the spectrum decomposition of the same range of wavelength. But the Raman band profiles are usually *intermediate* between Lorentzian and Gaussian profiles, also in the case of gases, and a Lorentzian profile is not automatically broadened into a Gaussian profile. This is evident from the several q-Gaussian fitted bands given by Sparavigna, 2023, 2024.

References

1. Al-Jishi, R., & Dresselhaus, G. (1982). Lattice-dynamical model for graphite. Physical Review B, 26(8), 4514.
2. Azzi, E. S., Karltun, E., & Sundberg, C. (2022). Life cycle assessment of urban uses of biochar and case study in Uppsala, Sweden. Biochar, 4(1), 18.
3. Beesley, L., Moreno-Jiménez, E., Gomez-Eyles, J. L., Harris, E., Robinson, B., & Sizmur, T. (2011). A review of biochars' potential role in the remediation, revegetation and restoration of contaminated soils. Environmental pollution, 159(12), 3269-3282.
4. Bernard, S., Beyssac, O., Benzerara, K., Findling, N., Tzvetkov, G., & Brown Jr, G. E. (2010). XANES, Raman and XRD study of anthracene-based cokes and saccharose-based chars submitted to high-temperature pyrolysis. Carbon, 48(9), 2506-2516.
5. Beyssac, O., Goffé, B., Petitet, J.-P., Froigneux, E., Moreau, M., & Rouzaud, J.-N. (2003). On the characterization of disordered and heterogeneous carbonaceous materials by Raman spectroscopy. Spectrochimica Acta Part A: Molecular Spectroscopy, 59, 2267−2276.
6. Beyssac, O., & Lazzeri, M. (2012). Application of Raman spectroscopy to the study of graphitic carbons in the Earth Sciences. in: Applications of Raman Spectroscopy to Earth Sciences and Cultural Heritage (J. Dubessy M.-C. Caumon and F. Rull editors). EMU Notes in Mineralogy 12, 415-454.
7. Bömmel, H., Li-Weber, M., Serfling, E., & Duschl, A. (2000). The environmental pollutant pyrene induces the production of IL-4. Journal of allergy and clinical immunology, 105(4), 796-802.
8. Bree, A., Kydd, R. A., Misra, T. N., & Vilkos, V. V. B. (1971). The fundamental frequencies of pyrene and pyrene-d10. Spectrochimica Acta Part A: Molecular Spectroscopy, 27(11), 2315-2332.
9. Brunetto, R., Pino, T., Dartois, E., Cao, A. T., d'Hendecourt, L., Strazzulla, G., & Bréchignac, P. (2009). Comparison of the Raman spectra of ion irradiated soot and collected extraterrestrial carbon. Icarus, 200(1), 323-337.
10. Campbell, I., & Fauchet, P. (1986). The effects of microcrystal size and shape on the one phonon Raman spectra of crystalline semiconductors. Solid State Commun. 1986, 58, 739−741.
11. Cayuela, M. L., Van Zwieten, L., Singh, B. P., Jeffery, S., Roig, A., & Sánchez-Monedero, M. A. (2014). Biochar's role in mitigating soil nitrous oxide emissions: A review and meta-analysis. Agriculture, Ecosystems & Environment, 191, 5-16.
12. Demtröder, W. (1982). Laser spectroscopy (Vol. 2). Berlin, Heidelberg: Springer.

13. Dippel, B., Jander, H., & Heintzenberg, J. (1999). NIR FT Raman spectroscopic study of flame soot. Physical Chemistry Chemical Physics, 1(20), 4707-4712.
14. Dresselhaus, M. S., Dresselhaus, G., Saito, R., & Jorio, A. (2005). Raman spectroscopy of carbon nanotubes. Physics reports, 409(2), 47-99.
15. Ferrari, A. C., & Robertson, J. (2000). Interpretation of Raman spectra of disordered and amorphous carbon. Phys. Rev. B, 61, 14095−14107.
16. Figueira-Duarte, T. M., & Mullen, K. (2011). Pyrene-based materials for organic electronics. Chemical reviews, 111(11), 7260-7314.
17. Gavilan, L., Ricketts, C. L., Bejaoui, S., Ricca, A., Boersma, C., Salama, F., & Mattioda, A. L. (2022). Raman spectroscopic study of pyrene in cosmic dust analogues: evolution from the gas to the solid phase. ACS Earth and Space Chemistry, 6(9), 2215-2225.
18. Godlewska, P., Ok, Y. S., & Oleszczuk, P. (2021). The dark side of black gold: Ecotoxicological aspects of biochar and biochar-amended soils. Journal of hazardous materials, 403, 123833.
19. Gu, X., Tian, S., Zhou, Q., Adkins, J., Gu, Z., Li, X., & Zheng, J. (2013). SERS detection of polycyclic aromatic hydrocarbons on a bowl-shaped silver cavity substrate. Rsc Advances, 3(48), 25989-25996.
20. Hanel, R., Thurner, S., & Tsallis, C. (2009). Limit distributions of scale-invariant probabilistic models of correlated random variables with the q-Gaussian as an explicit example. The European Physical Journal B, 72(2), 263.
21. Inoue, J., Yoshie, A., Tanaka, T., Onji, T., & Inoue, Y. (2017). Disappearance and alteration process of charcoal fragments in cumulative soils studied using Raman spectroscopy. Geoderma, 285, 164-172.
22. Jawhari, T., Hendra, P. J., Willis, H. A., & Judkins, M. (1990). Quantitative analysis using Raman methods. Spectrochimica Acta Part A: Molecular Spectroscopy, 46(2), 161-170.
23. Lee, S. C., Kitamura, Y., Chien, C. C., Cheng, C. S., Cheng, J. H., Tsai, S. H., & Hsieh, C. C. (2022). Development of Meso-and Macro-Pore Carbonization Technology from Biochar in Treating the Stumps of Representative Trees in Taiwan. Sustainability, 14(22), 14792.
24. Lehmann, J., & Joseph, S. (Eds.). (2015). Biochar for environmental management: science, technology and implementation. Routledge.
25. Mattioda, A. L., Gavilan, L., Ricketts, C. L., Najeeb, P. K., Ricca, A., & Boersma, C. (2024). The NASA Raman spectroscopic database: Ramdb version 1.00. Icarus, 408, 115769.
26. Richter, H.; Wang, Z. P.; Ley, L. The one phonon Raman spectrum in microcrystalline silicon. Solid State Commun. 1981, 39, 625−629.
27. Sadezky, A., Muckenhuber, H., Grothe, H., Niessner, R., & Pöschl, U. (2005). Raman microspectroscopy of soot and related carbonaceous materials: Spectral analysis and structural information. Carbon, 43(8), 1731-1742.
28. Smith, M. W., Dallmeyer, I., Johnson, T. J., Brauer, C. S., McEwen, J. S., Espinal, J. F., & Garcia-Perez, M. (2016). Structural analysis of char by Raman spectroscopy: Improving band assignments through computational calculations from first principles. Carbon, 100, 678-692.
29. Sohi, S. P. (2012). Carbon storage with benefits. Science, 338(6110), 1034-1035.
30. Sousa, D. V. D., Guimarães, L. M., Felix, J. F., Ker, J. C., Schaefer, C. E. R., & Rodet, M. J. (2020). Dynamic of the structural alteration of biochar in ancient Anthrosol over a long timescale by Raman spectroscopy. PloS one, 15(3), e0229447
31. Sparavigna, A. C. (2023). Multifunctional porosity in biochar. Int. J. Sciences, 7, 41-54.
32. Sparavigna, A. C. (2023). q-Gaussian Tsallis Line Shapes and Raman Spectral Bands. Int. J. Sciences, 12(3), 27-40, 2023, Available at SSRN: https://ssrn.com/abstract=4398623
33. Sparavigna, A. C. (2023). q-Gaussian Tsallis Line Shapes and Raman Spectral Bands. International Journal of Sciences, 12(03), 27-40. http://dx.doi.org/10.18483/ijSci.2671
34. Sparavigna, A. C. (2023). q-Gaussian Tsallis Line Shapes for Raman Spectroscopy (June 7, 2023). SSRN Electronic Journal. http://dx.doi.org/10.2139/ssrn.4445044

35. Sparavigna A. C. (2023). Tsallis q-Gaussian function as fitting lineshape for Graphite Raman bands. ChemRxiv. Cambridge: Cambridge Open Engage; 2023.
36. Sparavigna, A. C. (2023). SERS Spectral Bands of L-Cysteine, Cysteamine and Homocysteine Fitted by Tsallis q-Gaussian Functions. International Journal of Sciences, 12(09), 14–24. https://doi.org/10.18483/ijsci.2721
37. Sparavigna, A. C. (2024). Raman Spectroscopy of Siderite with q-Gaussian and split-q-Gaussian Analyses. International Journal of Sciences, 13(02), 8-21.
38. Tagliaferro, A., Rovere, M., Padovano, E., Bartoli, M., & Giorcelli, M. (2020). Introducing the novel mixed gaussian-lorentzian lineshape in the analysis of the raman signal of biochar. Nanomaterials, 10(9), 1748.
39. Tsallis, C. (1988). Possible generalization of Boltzmann-Gibbs statistics. Journal of statistical physics, 52, 479-487.
40. Tuinstra, F., & Koenig, J. L. (1970). Raman spectrum of graphite. The Journal of chemical physics, 53(3), 1126-1130.
41. Vinogradoff, V., Le Guillou, C., Bernard, S., Binet, L., Cartigny, P., Brearley, A. J., & Remusat, L. (2017). Paris vs. Murchison: Impact of hydrothermal alteration on organic matter in CM chondrites. Geochim. Cosmochim. Acta, 212, 234−252.
42. Wang, N., Chang, Z. Z., Xue, X. M., Yu, J. G., Shi, X. X., Ma, L. Q., & Li, H. B. (2017). Biochar decreases nitrogen oxide and enhances methane emissions via altering microbial community composition of anaerobic paddy soil. Science of the Total Environment, 581, 689-696.
43. Zhu, X., Chen, B., Zhu, L., & Xing, B. (2017). Effects and mechanisms of biochar-microbe interactions in soil improvement and pollution remediation: a review. Environmental pollution, 227, 98-115.